Direct Kinematics of a Double Parallel Robot Arm for Real Time Velocity Control

Min Ki Lee* and Kun Woo Park**

(*Received March 26, 1997*)

The determination of the direct kinematics of a parallel mechanism is a difficult problem but must be solved for practical application. This paper presents the efficient formulation of the direct kinematics and the Jacobian of a double parallel robot arm for velocity control. The robot arm consisls of two parallel mechanisms, and a central axis that generates positional and orientational motions independently. Given a set of lengths for the linear actuators, the direct kinematics computes the position and orientation of the end-effector, and the Jacobian transforms the velocities of the end-effector to those of the linear actuators. The developed formulation is implemented in a real-time control setting and its efficiency is demonstrated.

Key Words: Double Parallel Mechanism, Direct Kinematics, Geometric Constraint, Link Train, Active and Passive Joints, Jacobian, Computational Time, Velocity Control, Workspace.

1. Introduction

In previous researches the design and construction of a Double Parallel Robot Arm (DPRA), its inverse kinematics (Lee, 1995a) and dynamics (Lee, 1995b) have been studied. In this paper, the direct kinematics and Jacobian will be derived for velocity control. A six Degree-of-Freedom Parallel Manipulator, PM referred to as a Stewart Platform (SP), has six legs forming multiple closed loops and yielding highly nonlinear equations for the direct kinematics with multiple solu tions (Innocenti and Parenti-Casteui, 1990; Merlet 1993). Due to the complexity, Sugimoto (Sugimoto, 1987) presented a numerical solution method, while Raghavan (Raghavan, 1991) derived a set of Geometric Constraint (GC) equations to solve for the roots, and Merlet (Merlet, 1993) described the position representation in terms of the orientation to reduce the order of the GC equations ; their roots are convergent only in limited ranges, however. To simplify the GC equations, extra sensors are installed at passive joints to measure the GC motions (Cheok, Overholt, and Beck, 1993). However, adding sensors increases the possibility of link interference that, in turn, causes a reduction in the useful volume of the workspace. Therefore, the position and orientation are decoupled to diminish the order of the equations by a minimum number of sensors (Baron and Angeles, 1994 ; Zanganeh and Angeles, 1995).

In this paper, we separate the direct kinematics of the DPRA into a positional and an orientational part without adding any extra sensors, i. e., in the first PM, the GC equations for position are derived for a set of three lengths of legs, whereas in the second PM the GC equations for orientation are derived for a set of two lengths of legs. Since the order of the GC equations is only two or three, the computation solving for the roots of the equations is greatly reduced. Moreover, from the simplified DPRA, we find the approximate roots, which are close to the real ones, and substitute them as initial values of the Newton iterative method for a high rate of conver-

* Department of Control and Instrumentation Engr.

** Changwon National Univ. Sarim-dong 9, Changwon city, Kyungnam, Korea(e-mail : minkilee @sarim. changwon. ac. kr)

gence.

The real time direct kinematics is applied for velocity control. We must derive the Jacobian which can transform the given velocities of the end effector to those of the linear actuators. Screw theory (Mohamed and Duffy, 1985) has been applied to a Stewart Platform, and a 6×6 square Jacobian matrix is found to transform six components of velocities (linear and angular velocity) of the platform to those of the six linear actuators. But in the DPRA, two or three links support the platforms, so that the six components of the velocity of each PM cannot be directly transformed due to a non-square jacobian. This paper uses motor vector algebra (Sugimoto, 1987) to transform velocities, and combines them to find the Jacobian. The direct kinematics and the Jacobian are implemented in a real time control setting to evaluate the performance of the DPRA.

2. Geometric Modeling of the DPRA

As shown in Fig. 1, for i=1, ···, 5, leg_i is connected from B_i to P_i, which are placed at the base and platform, respectively. $B_{i(i=1,2,3)}$ and $P_{i(i=1,2,3)}$ are located symmetrically 120° apart and $\|\overrightarrow{O_0B_i}\|=r_{B1}$ and $\|\overrightarrow{O_3P_i}\|=r_{P1}$, while $B_{i(i=4,5)}$ and $P_{i(i=4,5)}$ make angles ζ_1 and ζ_2 with the horizontal, respectively, and $\|\overrightarrow{O_2B_i}\|=r_{B2}$ and $\|\overrightarrow{O_5P_i}\|=r_{P2}$. $O_{i(i=0,2,3,5)}$ are the central points of the base and the platform. Leg_i are the link train of U_{i1}-n_{i1}-PR_{i2}-n_{i2}-U_{i3} as shown in Fig. 2. Universal joints U_{i1} provide 2-Degree-Of-Freedom (DOF) in θ_{i1} and θ_{i2}, while prismatic and rotary joints PR_{i2} give another 2-DOF in θ_{i3} and θ_{i4}. Finally, 2-DOF corresponding to θ_{i5} and θ_{i6} are added by universal joints U_{i3}. $\theta_{i(j=1,2,4,5,6)}$ are all passive joints but the active joint θ_{i3} shortens or extends the length of $\overrightarrow{B_iP_i}$ by means of a Linear Actuator (LA_i). To increase the range of the universal

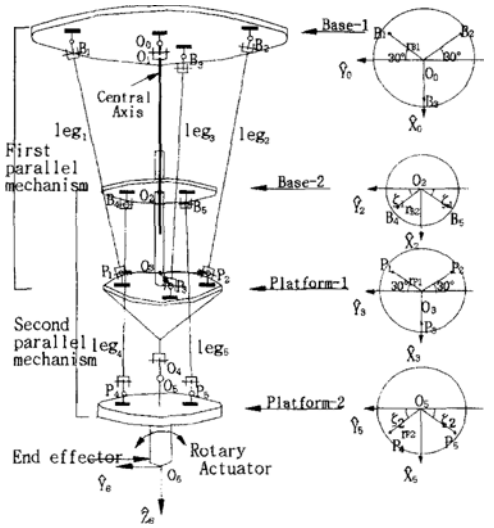

Fig. 1 Double Parallel Robot Arm.

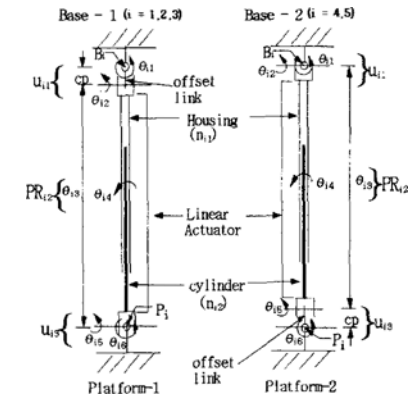

Fig. 2 Linear Actuators and joints of Leg_i.

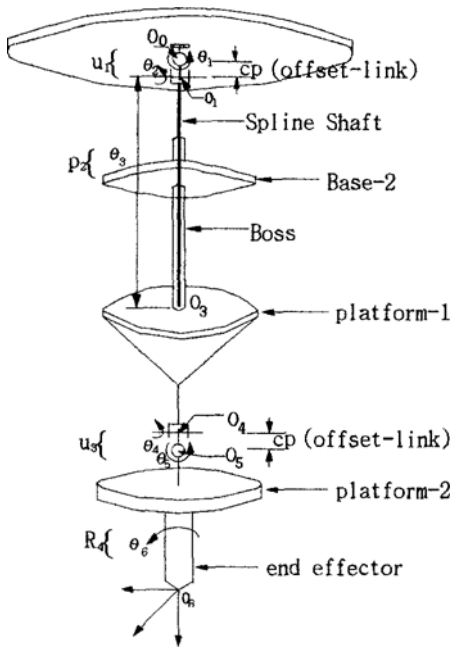

Fig. 3 Central Axis.

joints, offset links are inserted in the upper joints $U_{i1(i=1,2,3)}$ of the first PM and the lower joint $U_{i3(i=4,5)}$ of the second PM. To avoid singularites (Gosselin and Angeles 1990), the direction of joints θ_{i1} are mutually perpendicular to those of the lower joints θ_{i2}, while the directions of θ_{i6} are perpendicular to the upper joints θ_{i5} for i=1, ···, 5.

A central axis is the link train composed of all passive joints as shown in Fig. 3. In the center of Base-1 is located the central axis which constrains Platform-1 to rotary motions θ_1 and θ_2 by a universal joint U_1, and the sliding motion θ_3 by a prismatic joint P_2. Platform-2 is also constrained to rotary motions θ_4 and θ_5 by a universal joint U_3. $\theta_{i(i=1,2,3)}$, which position the Platform-1, are driven by the GC of the first PM and the active joints $\theta_{i3(i=1,2,3)}$ while $\theta_{i(i=4,5)}$, which orient the Platform-2, are driven by the GC of the second PM and the $\theta_{i3(i=4,5)}$. Therefore, the position and the orientation motions of the DPRA are independently generated and decoupled from each other. For a six DOF link train, an active joint R_4 is mounted on Platform-2 to yield a rotary motion θ_6. Consequently, the central axis including joint R_4 is considered as a six DOF serial manipulator.

To analyze the joint motions of the central axis, we assign coordinates {i} to points O_i for i=0, 1, ···, 6 as shown in Fig. 1. For a given position and orientation of {6} relative to {0}, the joint displacements of the central axis are obtained by

$$(\overrightarrow{{}^0O_0O_6},\ {}^0R_6) = Kin\_center(\theta_1,\ \cdots,\ \theta_6) \quad (1)$$

where $\overrightarrow{{}^0O_0O_6}$ is the position vector and ${}^0R_6$ is a 3 ×3 rotation matrix. The left superscript indicates the coordinate which describes the position vector or the rotation matrix. $Kin\_center(\cdot)$ is the direct kinematics of the central axis, which is identical to that of a serial manipulator. In the DPRA, the positions and orientations of coordinates {3} and {5} are decoupled by

$$(\overrightarrow{{}^0O_0O_3},\ {}^0R_3) = Kin\_center(\theta_1,\ \theta_2,\ \theta_3) \quad (2)$$

$$(\overrightarrow{{}^2O_2O_5},\ {}^2R_5) = Kin\_center(\theta_4,\ \theta_5) \quad (3).$$

The GC displacements $\theta_{i(i=1,\cdots,5)}$ of the central axis involved in the above equations can also be independently described by

$$\theta_i = first\_const\_i(\theta_{13},\ \theta_{23},\ \theta_{33}) \quad (i=1,\ 2,\ 3) \quad (4)$$

$$\theta_i = second\_const\_i(\theta_{43},\ \theta_{53}) \quad (i=4.\ 5) \quad (5)$$

The direct kinematics problem is to find $first\_const\_i(\cdot)$ and $second\_const\_i(\cdot)$, which are the first and the second GC equations, respectively, using the GC conditions in each PM. Notice that the equations are a function of two or three lengths, so their orders are lower than those of the SP (Raghavan, 1991). If are measure the joints of the central axis with extra sensors, we can directly obtain the direct kinematics by Eq (1).

3. Geometric Constraint Equations

In order to derive the GC equations, we find the closed loops the first and second PM. Three loops of $O_0B_1P_1O_3$, $O_0B_2P_2O_3$ and $O_0B_3P_3O_3$ are involved in the first PM, and two loops of $O_2B_4P_4O_5$ and $O_2B_4P_5O_5$ in the second PM. Position vectors $\overrightarrow{{}^0O_0B_i}$ and $\overrightarrow{{}^3O_3P_i}$ of the closed loop in the first PM are

$$\overrightarrow{{}^0O_0B_1} = \{-\frac{r_{B1}}{2},\ \frac{\sqrt{3}}{2}r_{B1},\ 0\},$$

$$\overrightarrow{{}^0O_0B_2} = \{-\frac{r_{B1}}{2},\ -\frac{\sqrt{3}}{2}r_{B1},\ 0\},$$

$$\overrightarrow{{}^0O_0B_3} = \{r_{B1},\ 0,\ 0\} \quad (6a)$$

and

$$\overrightarrow{{}^3O_3P_1} = \{-\frac{r_{P1}}{2},\ \frac{\sqrt{3}}{2}r_{P1},\ 0\},$$

$$\overrightarrow{{}^3O_3P_2} = \{-\frac{r_{P1}}{2},\ -\frac{\sqrt{3}}{2}r_{P1},\ 0\},$$

$$\overrightarrow{{}^3O_0P_3} = \{r_{P1},\ 0,\ 0\} \quad (6b)$$

From Eq. (2), we can write

$$\overrightarrow{{}^0O_0O_3} = \{\theta_3 s\theta_2,\ -s\theta_1(cp+\theta_3 c\theta_2),\ c\theta_1(cp+\theta_3 c\theta_2)\} \quad (7)$$

and from $Kin\_leg\_i(\theta_{i1},\ \theta_{i2},\ \theta_{i3})$, which is the direct kinematics of leg_i, we get

$$\overrightarrow{{}^0B_iP_i} = \{\theta_{i3}s\theta_{i2},\ -s\theta_{i1}(cp+\theta_{i3}c\theta_{i2}),\ c\theta_{i1}(cp+\theta_{i3}c\theta_{i2})\} \quad (8).$$

Since $\overrightarrow{{}^0O_0O_3}$ is located in the center of Platform -1, and B_i and P_i are symmetrically 120° apart, the relations between $\overrightarrow{B_iP_i}$ and $\overrightarrow{{}^0O_0O_3}$ is

$$\overrightarrow{{}^0O_0O_3} = 1/3\sum_{i=1}^{3}\overrightarrow{{}^0B_iP_i} \quad (9).$$

The above equation represents three GC relations

including nine unknowns such as θ_i, θ_{i1} and θ_{i2} for i=1, 2, 3. Thus we need six more GC relations as follows : from the closed loops $O_0O_3P_1B_1$ and $O_0O_3P_2B_2$, $\overrightarrow{{}^0P_1P_2}$ is determined by

$$\overrightarrow{{}^0P_1P_2}=(\overrightarrow{{}^0O_0B_2}+\overrightarrow{{}^0B_2P_2})-(\overrightarrow{{}^0O_0B_1}+\overrightarrow{{}^0B_1P_1})$$
$$={}^0R_3(\overrightarrow{{}^3O_3P_2}-\overrightarrow{{}^3O_3P_1}) \quad (10)$$

Correspondingly, from the closed loops $O_0O_3P_2B_2$ and $O_0O_3P_3B_3$, $\overrightarrow{{}^0P_2P_3}$ is

$$\overrightarrow{{}^0P_2P_3}=(\overrightarrow{{}^0O_0B_3}+\overrightarrow{{}^0B_3P_3})-(\overrightarrow{{}^0O_0B_2}+\overrightarrow{{}^0B_2P_2})$$
$$={}^0R_3(\overrightarrow{{}^3O_3P_3}-\overrightarrow{{}^3O_3P_2}) \quad (11)$$

To simplify the equations, the following variables are defined :

$$cb_i=\theta_{i3}\ c\theta_{i2},\ sb_i=\theta_{i3}\ s\theta_{i2}$$
$$ss_i=(cp+cb_i)\,s\theta_{i1},\ cc_i=(cp+cb_i)\,c\theta_{i1}$$

where $c(\cdot)=\cos(\cdot)$ and $s(\cdot)=\sin(\cdot)$. Substituting the variables into GC Eqs. (9)-(11), we solve for them.

Then the definition of ss_i and cc_i, yields

$$cb_i=\pm\sqrt{ss_i^2+cc_i^2}-cp \quad (12)$$

If $-90°<\theta_{i2}<90°$, cb_i are always positive. So, we can take only a positive square root for a unique solution. Referring to $cb_i^2+sb_i^2=\theta_{i3}^2$, three GC equations are derived by

$$cf_i=sb_i^2+cb_i^2-\theta_{i3}^2=0 \ (i=1,\ 2,\ 3) \quad (13)$$

These are the third order simultaneous equations given in the Appendix to compute the joint displacements of the central axis for a set of $\theta_{i3(i=1,2,3)}$. *second_const_i*$(\cdot)$ is also derived from the GC motions of the closed loops in the second PM. When $l_2=\|\overrightarrow{O_2O_4}\|$, $\overrightarrow{{}^2O_2O_5}$ obtained from Eq. (3) is converted to

$$\overrightarrow{{}^5O_5O_2}=-{}^5R_2\,\overrightarrow{{}^2O_2O_5}=\{l_2s\theta_4,\ -s\theta_5(cp+l_2c\theta_4),\ -c\theta_5(cp+l_2c\theta_4)\} \quad (14)$$

From the direct kinematics of *Kin_leg_i*$(\theta_{i3},\ \theta_{i5},\ \theta_{i6})$, we can write

$$\overrightarrow{{}^5P_iB_i}=\{\theta_{i3}s\theta_{i6},\ -s\theta_{i5}(cp+\theta_{i3}s\theta_{i6}),\ -c\theta_{i5}(cp+\theta_{i3}c\theta_{i6})\} \quad (15)$$

Also, from the closed loops $O_2O_5P_4B_4$ and $O_2O_5P_5B_5$, $\overrightarrow{{}^5P_iB_i}$ can be expressed as

$$\overrightarrow{{}^5P_iB_i}=\overrightarrow{{}^5O_5O_2}+{}^5R_2\,\overrightarrow{{}^2O_2B_i}-\overrightarrow{{}^5O_5P_i} \ (i=4,\ 5) \quad (16)$$

Substituting Eq. (14) into Eq. (16) and solving for $s\theta_{i5(i=4,5)}$ and $c\theta_{i5(i=4,5)}$ of the resulting x-and y-component equations :

Restricting $-90°<\theta_{ij(j=5,6)}<90°$ for $c\theta_{ij}=+\sqrt{1-s\theta_{ij}^2}$ and substituting $c\theta_{ij}$ and $s\theta_{ij}$ into the z-components of Eq. (16), we get

$$cf_i=(\overrightarrow{{}^5P_iB_i})_{z-comp}-(\overrightarrow{{}^5O_5O_2}+{}^5R_2\,\overrightarrow{{}^2O_2B_i}-\overrightarrow{{}^5O_5P_i})_{z-comp}=0 \quad (i=4,\ 5) \quad (17)$$

The above equations are the second order GC equations given in the Appendix to compute $\theta_{i(i=4,5)}$ for a given set of $\theta_{i3(i=4,5)}$.

It is noted that the GC equations of the DPRA are expressed as second or third-order simultaneous equations, reducing the computation burden. Moreover, since the solution is unique by taking only a positive square root, we do not have to sort the solutions. However, the GC equations were not expressed in explicit form, so that Newton's numerical method is applied to find the roots of the equations. For better convergence, an approximate root close to a real root is obtained from the simplified DPRA and used as an initial value in the numerical method.

Simplifying the DPRA with cp=0, $r_{P1}=0$ and $r_{B2}=0$, we get the GC equations of the first and second PM as follows :

$$cf_1{}^0=\theta_3^2-\frac{r_{B1}\theta_3s\theta_1c\theta_2}{\sqrt{3}}+\frac{r_{B1}\theta_3s\theta_2}{3}+\frac{r_{B1}{}^2}{9}-\theta_{13}{}^2$$
$$cf_2{}^0=\theta_3^2-\frac{r_{B1}\theta_3s\theta_1c\theta_2}{\sqrt{3}}+\frac{r_{B1}\theta_3s\theta_2}{3}+\frac{r_{B1}{}^2}{9}-\theta_{23}{}^2 \quad (13)'$$
$$cf_3{}^0=\theta_3^2-\frac{2r_{B1}\theta_3s\theta_2}{3}+\frac{r_{B1}{}^2}{9}-\theta_{33}{}^2$$
$$cf_4{}^0=2l_2r_{P2}c\theta_4s\theta_5c\zeta_2-2l_2r_{P2}s\theta_4c\zeta_2+l_2{}^2+r_{P2}{}^2+r_{P2}{}^2c2\zeta_2-\theta_{43}{}^2$$
$$cf_5{}^0=-2l_2r_{P2}c\theta_4s\theta_5c\zeta_2-2l_2r_{P2}s\theta_4c\zeta_2+l_2{}^2+r_{P2}{}^2+r_{P2}{}^2c2\zeta_2-\theta_{53}{}^2 \quad (17)'$$

From the simplified equations, we solve for θ_i and let it be θ_i^0 to distinguish from the real roots. For the Newton iterative forms, the GC Eqs. (13) and (17) are written, respectively, as

$$F_1[X_1]=0,\ F_2[X_2]=0$$

where, $F_1=[cf_1\ cf_2\ cf_3]^T$, $F_2=[cf_4\ cf_5]^T$
$X_1=[\theta_1\ \theta_2\ \theta_3]^T$, $X_2=[\theta_4\ \theta_5]^T$

The classical Newton's method for the solution of the GC equations yields

$$X_p^{k+1}=X_p^k-\left[\frac{\partial F_p(X_p^k)}{\partial X_p}\right]^{-1}F_p(X_p^k) \quad (p=1, 2) \tag{18}$$

Here, $[\partial F_p(X_p^k)/\partial X_p]^{-1}$ requires much computations due to the matrix inversion operation. But if X_p^0 are substituted by the initial values $[\theta_1^0\ \theta_2^0\ \theta_3^0]^T$ or $[\theta_4^0\ \theta_5^0]^T$, they can be regarded as constant while converging (Merlet, 1993). Therefore, we let $J_p^{0-1}=[\partial F_p(X_p^k)/\partial X_p]^{-1}$ and repeat the iterative computation until the error becomes negligibly small. The iterative computation with constant matrices is never divergent except at the boundaries of the workspace where the initial values from the simplified DPRA are extremely different from the real roots. Once we find real roots $X_1=[\theta_1\ \theta_2\ \theta_3]^T$ and $X_2=[\theta_4\ \theta_5]^T$, we substitute θ_i (i=1, 2, ···, 5) and θ_6 into Eq.(1) to compute the position and orientation of the end-effector.

4. Velocity Control

The velocity control of the PM is performed in the tool base, so that we have to transform the velocities of the end effector to those of LA_i. In the DPRA, the six components of the velocity of the platform cannot be directly transformed by a square Jacobian matrix because only two or three legs are installed in each PM. We instead use a motor vector opproach to obtain the formulation for transforming velocities.

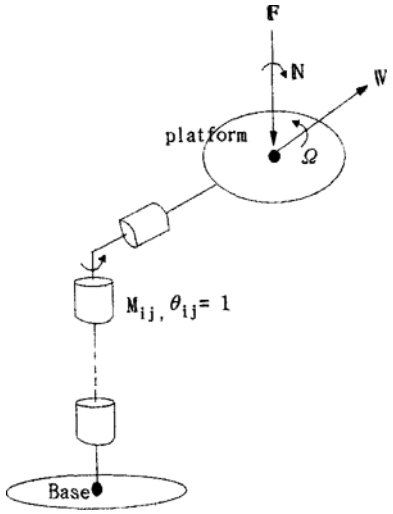

Fig. 4 Motor vector.

We depict a motor vector as shown in Fig. 4. When the j-joint θ_{ij} of link train i is actuated by unit velocity, the angular and linear velocities of the platform are Ω and V, respectively. Then the motor vector of joint j of link train i is defined by

$$M_{ij}=[\Omega \quad V]^T \tag{19}$$

With the motor vector, the velocity of the end effector of the DPRA, *Endvel_end*, can be expressed as

$$Endvel\_end=\dot{\theta}_1M_1+\cdots+\dot{\theta}_jM_j+\cdots+\dot{\theta}_6M_6 \tag{20}$$

where $\dot{\theta}_{i(i=1,2,\cdots,6)}$ are the joint velocities of the central axis and $M_{i(i=1,2,\cdots,6)}$ are the corresponding motor vectors. Let J_c be Jacobian matrix relating $\dot{\theta}_{i(i=1,2,\cdots,6)}$ to *Endvel_end*. We get

$$Endvel\_end=J_c\ \dot{\Theta} \tag{21}$$

where $J_c=[M_1\ M_2\cdots M_6]$ is a 6×6 matrix and $\dot{\Theta}=[\dot{\theta}_1\ \dot{\theta}_2\ \cdots,\ \dot{\theta}_6]^T$ is a 6×1 vector. $\dot{\theta}_6$ can be actively generated, but $\dot{\theta}_{i(i=1,2,\cdots,5)}$ must be driven by $\dot{\theta}_{i3}$ of LA_i$_{(i=1,2,\cdots,5)}$. To find $\dot{\theta}_{i3}$, the velocities of P$_{i(i=1,2,\cdots,5)}$ are computed as

$$Endvel\_P_i=\dot{\theta}_1{}^iM_1+\dot{\theta}_2{}^iM_2+\dot{\theta}_3{}^iM_3 \quad (i=1, 2, 3) \tag{22a}$$

$$Endvel\_P_i=\dot{\theta}_4{}^iM_4+\dot{\theta}_5{}^iM_5 \quad (i=4, 5) \tag{22b}$$

where ${}^iM_j$ are determined from the relations between the velocities of points P$_i$ and the unit velocities of the joints of a central axis. Also, *Endvel_P$_i$* can be obtained by motor vectors between P$_i$ and j-joints of leg_i, i. e.,

$$Endvel\_P_i=\dot{\theta}_{i1}{}^iM_{i1}+\dot{\theta}_{i2}{}^iM_{i2}+\dot{\theta}_{i3}{}^iM_{i3} \quad (i=1, 2, 3) \tag{23a}$$

$$Endvel\_P_i=\dot{\theta}_{i1}{}^iM_{i1}+\cdots+\dot{\theta}_{ij}{}^iM_{ij}+\cdots+\dot{\theta}_{i6}{}^iM_{i6} \quad (i=4, 5) \tag{23b}$$

Note that *Endvel_P$_i$* of the first PM is affected only by the velocities of the upper joints $\dot{\theta}_{ij(j=1,2,3)}$, but *Endvel_P$_i$* of the second PM is influenced by the velocities of $\dot{\theta}_{ij(j=1,2,3)}$ as well as the lower joints $\dot{\theta}_{ij(j=4,5,6)}$ because of the offset links inserted. Therefore, the ${}^iM_j$ and ${}^iM_{ij}$ of the first PM must be 3×1 motor vectors to compute the linear components of $Endvel\_P_{i(i=1,2,3)}$ whereas the ${}^iM_j$ and ${}^iM_{ij}$ of the second PM must be 6×1 motor vectors to obtain both angular and linear compo-

nents of $Endvel\_P_{i(i=4,5)}$. Let ${}^iJ_c=[{}^iM_1\ {}^iM_2\ {}^iM_3]$ for i=1, 2, 3, ${}^iJ_c=[{}^iM_4\ {}^iM_5]$ for i=4, 5, $\dot{\Theta}_f=[\dot{\theta}_1\ \dot{\theta}_2\ \dot{\theta}_3]^T$ and $\dot{\Theta}_s=[\dot{\theta}_4\ \dot{\theta}_5]^T$. Eq. (22) can be rewritten as

$$Endvel\_P_i={}^iJ_c\ \dot{\Theta}_f \quad (i=1, 2, 3) \tag{24a}$$
$$Endvel\_P_i={}^iJ_c\ \dot{\Theta}_s \quad (i=4, 5) \tag{24b}$$

When defining ${}^iJ_i=[{}^iM_{i1}\ {}^iM_{i2}\ {}^iM_{i3}]$ for i=1, 2, 3, and ${}^iJ_i=[{}^iM_{i1}\ {}^iM_{i2}\cdots{}^iM_{i6}]$ for i=4, 5, we can compute joint velocities of leg_i for a given $Endvel\_P_i$, i. e.,

$$\dot{\Theta}_i={}^iJ_i^{-1}\ Endvel\_P_i \quad (i=1, 2, 3) \tag{25a}$$
$$\dot{\Theta}_i={}^iJ_i^{-1}\ Endvel\_P_i \quad (i=4, 5) \tag{25b}$$

For velocity control, only the $\dot{\theta}_{i3}$ are chosen out of $\dot{\Theta}_i=[\dot{\theta}_{i1}\ \dot{\theta}_{i2}\ \dot{\theta}_{i3}]^T$ for i=1, 2, 3 or $\dot{\Theta}_i=[\dot{\theta}_{i1}\ \dot{\theta}_{i2}\ \dot{\theta}_{i3}\cdots\dot{\theta}_{i6}]^T$ for i=4, 5. When the row vectors of ${}^iJ_i^{-1}$ are defined as follows

$$[{}^iS_1^T\ {}^iS_2^T\ {}^iS_3^T]^T={}^iJ_i^{-1} \quad \text{for i=1, 2, 3}$$
$$[{}^iS_1^T\ {}^iS_2^T\ {}^iS_3^T\cdots{}^iS_6^T]^T={}^iJ_i^{-1} \quad \text{for i=4, 5}$$

the active joint velocity $\dot{\theta}_{i3}$ will be

$$\dot{\theta}_{i3}={}^iS_3\ Endvel\_P_i \tag{26}$$

Combining Eqs. (21), (24), (25) and (26) yields

$$[\dot{\theta}_{13}\ \dot{\theta}_{23}\ \dot{\theta}_{33}\ \dot{\theta}_{43}\ \dot{\theta}_{53}\ \dot{\theta}_6]^T=\mathrm{A}\ \mathrm{B}\ J_c^{-1}\ Endvel\_end \tag{27}$$

where A and B are 6×22 and 22×6 matrices, respectively. They are

$$\mathrm{A}=\begin{bmatrix} {}^1S_3 & & & & & 0_{(12\times3)} \\ & {}^2S_3 & & & & \\ & & {}^3S_3 & & & \\ & & & {}^4S_3 & & \\ 0_{(9\times2)} & & & & {}^5S_3 & \\ & & & & & 1 \end{bmatrix},$$

$$\mathrm{B}=\begin{bmatrix} {}^1J_c & & & & \\ {}^2J_c & 0_{(9\times3)} & & & \\ {}^3J_c & & & & \\ & & {}^4J_c & & \\ 0_{(12\times3)} & & {}^5J_c & & \\ & & & 1 & \end{bmatrix}$$

and, the Jacobian, which is a 6×6 square matrix, is

$$\mathrm{J}=\mathrm{A}\ \mathrm{B}\ J_c^{-1} \tag{28}$$

The Jacobian requires considevable computation because of the offset links. If they are short enough to be negligible, we can directly compute ${}^iS_3$ by projecting $Endvel\_P_i$ in the direction of LA_i, i. e.,

$${}^iS_{s3}=\frac{\overrightarrow{B_iP_i}}{\|\overrightarrow{B_iP_i}\|} \tag{29}$$

${}^iS_{s3}$, which are simplified vectors of ${}^iS_3$, can reduce the computation i.e., the inverse matrices included in matrix A. Also, ${}^iS_{s3}$ are always 3×1 vectors so that only the linear components of $Endvel\_P_{i(i=4,5)}$ are necessary. Therefore, ${}^iM_{j(i,j=4,5)}$ and ${}^iM_{ij(i,j=4,5)}$ are 3×1 motor vectors and ${}^iJ_{c(i=4,5)}$ are defined by 3×2 matrices, i. e.,

$${}^iJ_{sc}=[{}^iM_{s4}\ {}^iM_{s5}] \quad (i=4, 5) \tag{30}$$

The Jacobian is simplified to

$$\mathrm{J_s}=\mathrm{A_s}\ \mathrm{B_s}\ J_c^{-1} \tag{28}'$$

where A_s and B_s are a 6×16 and a 16×6 matrices, respectively.

The Jacobian requires passive joint displacements of a central axis and leg_i, which should be computed by the direct kinematics. Thus, the real time direct kinematics and the Jacobian must be implemented as shown in Fig. 5.

The controller sets up $Endvel\_end$, and computes initial values from the simplified GC equations with the measured θ_{i3}. The initial values are

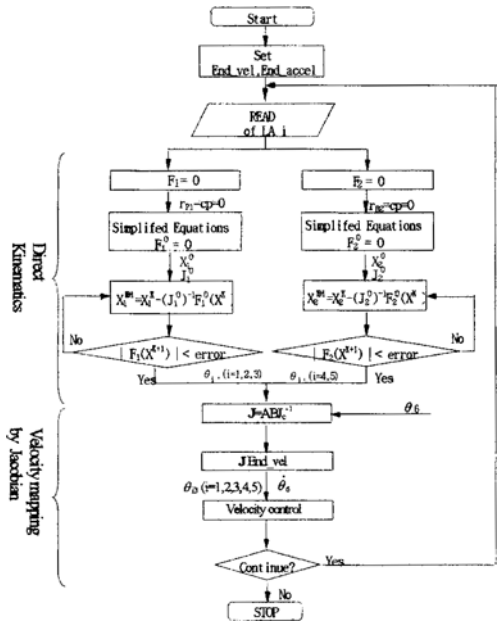

Fig. 5 Flow chart of velocity control.

Table 1 Computational time of velocity control.

Step	Process		Computation Time(m-sec)	
1	Initial Value X_p^0, J_p^0		0.08	
2	Newton's Iteration $\|F_p(X_p^{k+1})\| < error$		2.09	
3	Direct Kinematics of Central Axis *kin_center* $(\theta_1, \theta_2, \cdots, \theta_6)$		0.25	
4	J_c^{-1}		0.40	
	Velocity obtained by Full Jacobian	Computation Time (m-sec)	Velocity obtained by Simplified Jacobian	Computation Time (m-sec)
5	A	3.01	A_s	0.11
6	B	0.82	B_s	0.66
7	ABJ_c^{-1}	0.99	$A_sB_sJ_c^{-1}$	0.71
Total		7.64		4.3

substituted into Newton's method and the convergent roots are obtained by iterative computation. With the obtained roots, the direct kinematics of the central axis computes the position and the orientation of an end effector. We compute the Jacobian matrix and transform the *Endvel_end* to the θ_{i3}. They are converted to velocity commands and sent to servo motors to execute the velocity control. The controller follows the above steps until the stop key is pressed.

Table 1 presents the computational time of each step for velocity control. A total time of 7.64 m-sec is fast enough for real time control, but the burden of computation is caused by the A and B with the offset links. If A_s and B_s are applied, the computational time is reduced to 4.3 m-sec. The results of velocity control show that the simplified Jacobian produces better performance than the real ones from fast computations.

5. Construction of DPRA and Analytical Results

We constructed the DPRA for a grinding robot as shown in Fig. 6. The payload is 100kg with a weight of 150kg, the sliding ranges of the LA_i are $754\text{mm} < \theta_{i3}(i=1, 2, 3) < 1128\text{mm}$, $630\text{mm} < \theta_{i3}(i=4, 5) < 800\text{mm}$, and the range of the rotary actuator is $-180° < \theta_6 < 180°$. The sliding motions

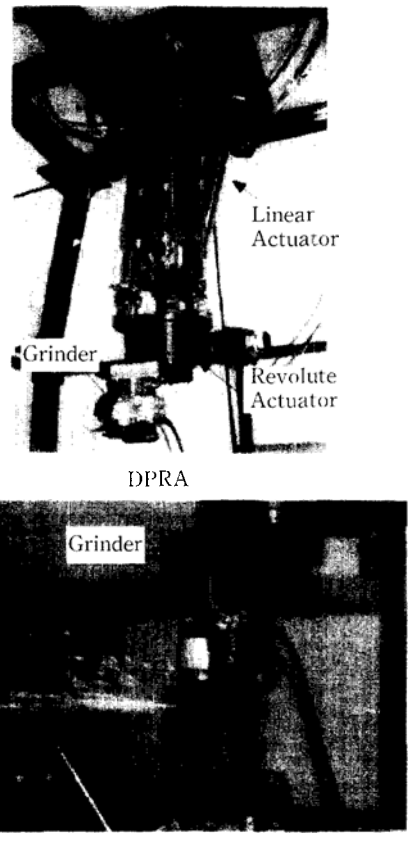

Fig. 6 Grinding Robot System using the DPRA (Constructed in Changwon National University).

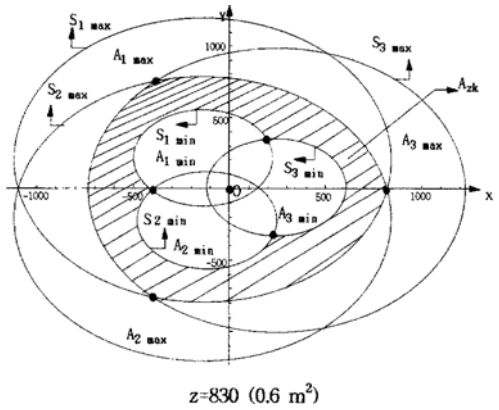

Fig. 7 The section of Positional Workspace of the DPRA.

are generated by ball screws with 5mm leads, while the rotating motion is from the worm gear whose reduction ratio is 1/90. Design parameters are $r_{B1}=250$, $r_{P1}=80$, $r_{B2}=80$, $r_{P2}=150$, cp=20, $\zeta_1=20°$ and $\zeta_2=45°$.

Figure 7 depicts the section of the positional workspace with the z- plane. The positional workspace is the volume which the Platform-1 can reach when the lengths of LA_i$_{(i=1,2,3)}$ are changed from the minimum to maximum. The section consists of areas, $A_{i\ min}$ and $A_{i\ max}$, closed by $S_{i\ min}$ and $S_{i\ max}$ which are the curves of the x-y positions of the Platform-1 placed by maximum and minimum lengths. Reachable positions are located inside all $A_{i\ max}$ and outside all $A_{i\ min}$, so that the section of the workspace is the intersection of 3 annular regions.

The volume of the workspace of the DPRA is approximately equal to 0.3664m^3.

The orientational workspace is defined as the pose of Platform-2 with respect to Base-2, which is (θ_4, θ_5), generated by the LA_i $_{(i=4,5)}$. Fig. 8 shows $S_{i\ min}$ and $S_{i\ max}$, which are the curves of the $\theta_4-\theta_5$ angles of the Platform-2, generated by minimum and maximum lengths. The orientational workspace is the intersection of the two regions between $S_{i\ min}$ and $S_{i\ max}$ for i=4 and 5. The result shows that the ranges of θ_4 and θ_5 are more than 60°.

To demonstrate the advantage in workspace, the workspace is compared with that of the SP in which the leg_i$_{(i=1,2,\cdots,6)}$ are installed between Base

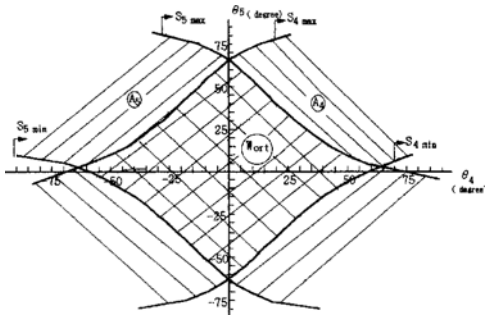

Fig. 8 The section of Orientational Workspace of the DPRA.

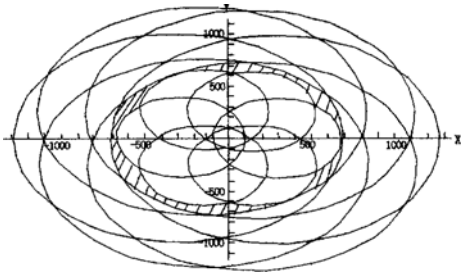

Fig. 9 The Section of Positional Workspace of Stewart Platform.

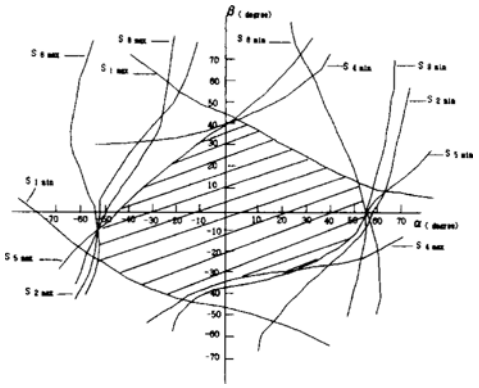

Fig. 10 The Section of Orientational Workspace of Stewart Platform.

-1 and Platform-1 without a central axis. All the design parameters of the leg_i are the same as those of the DPRA. For the minimum and maximum lengths of LA_i $_{(i=1,2,\cdots,6)}$, closed curves of $S_{i\ min}$ and $S_{i\ max}$ are shown in Fig. 9. The section of the workspace is the intersection of 6 annular regions and the volume of the workspace of the SP is 0.330m^3.

The orientational workspace is compared with

that of the SP. Here the roll of the DPRA is not sonsidered because its driving mechanism is different from that of the SP. We define (α, β) representing the yaw and pitch motions which are the pose of the platform with respect to the base. As shown in Fig. 10, twelve curves $S_{i\ \min}$ and $S_{i\ \max}$ for i=1, 2, ···, 6, are obtained on the α-β plane determined at the minimum and maximum lengths of LA_i. The orientational workspace is below 50°. It is the intersection of six regions between $S_{i\ \min}$ and $S_{i\ \max}$. The comparison of the workspace shows that the increase in the number of legs between bases and platforms increases link interference and decreases the workspace.

An array of points of O_3 is plotted for positional workspace as in Fig. 11, and the rotations of $\theta_{i(i=4,5)}$ are for an orientational workspace as in Fig. 12.

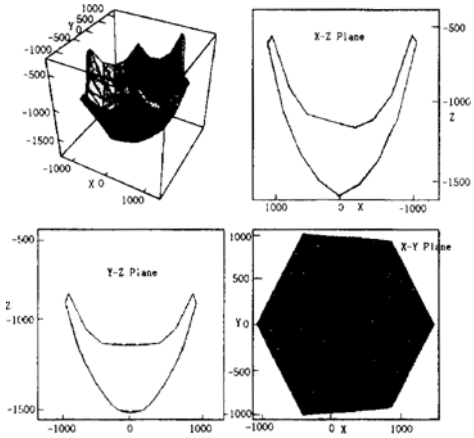

Fig. 11 Positional Workspace.

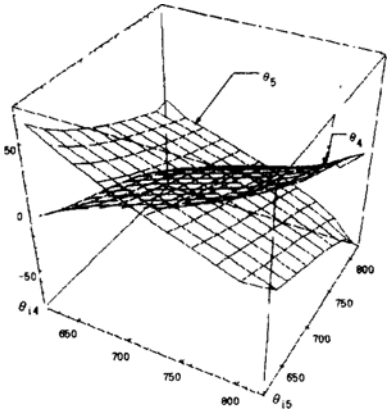

Fig. 12 Orientational Workspace.

The $\theta_{3(i=1,2,3)}$ generate the positional workspace whose height and width are 1000mm and 2000mm, respectively, excluding the regions of interferences. At any interior position, the orientational workspace is independently generated by the $\theta_{3(i=4,5)}$ and its ranges are from $-60°$ to 60°, respectively. This solves a major problem in workspace of the parallel mechanism.

The velocity control is executed by implementing the direct kinematics and the Jacobian. When we move the robot from {{−600, 0, 1200}, {0, 0, 0}} to {{600, 0, 1200}, {0, 0, 0}} with *Endvel_end* =200mm/sec, the velocity profiles of the end effector and the LA_i are shown in Fig. 13. Correspondingly, Fig. 14 depicts the position profiles in the x-y and x-z planes. The LA_i accelerates and decelerates the DPRA in 0.1 second even with the large payload of 50kg. This

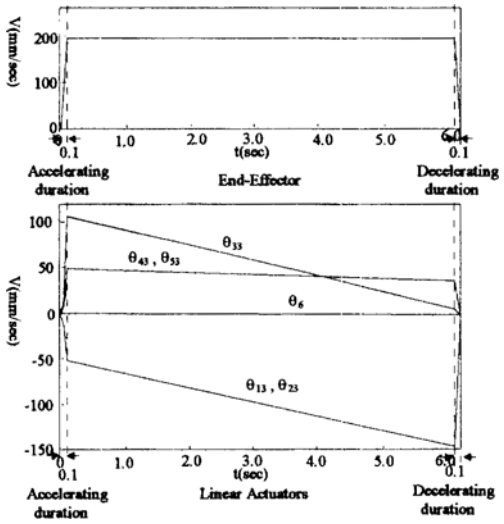

Fig. 13 Velocity Profiles of the End-Effector and Linear Actuator.

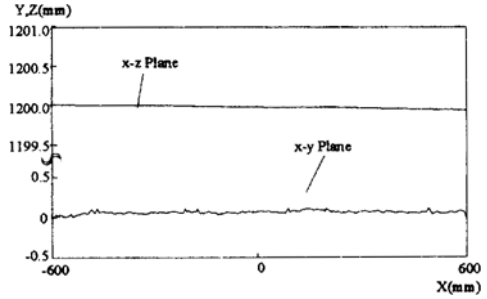

Fig. 14 Position Profiles of the End-Effector.

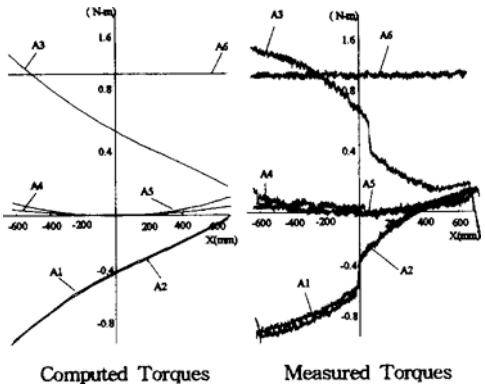

Fig. 15 The computed and measured torques acting at the motors of linear actuators.

demonstrates that the dynamic response is very fast due to the small inertia of the parallel mechanism.

During velocity control, the end effector deviates from the desired path within 0.1 mm, but these deviations are acceptable for deburring work. The deviations are precisely influenced by the computational times of the direct kinematics and the Jacobian. If there is long delay in transforming the velocities, the velocity commands cannot be rapidly generated at the current position. Therefore, the simplified Jacobian yields better performance than the real Jacobicn even though there are errors in the velocity commands by ignoring the offset links. To reduce the deviations, we control the position of the end effector by position control, which is easily implemented by the inverse kinematics.

Figure 15 shows the computed torques by the Jacobian and the measurment acting at the motors of LA_i when the grinding force and moment are 300N and 60N-m, respectively, and the payload is 50kg. The torques are less than 1.6N-m, so that the DPRA can be constructed with small motors for a high ratio of payload to weight and low power dissipation.

6. Conclusion

This paper developed algorithms for the direct kinematics and the Jacobian of a double parallel robot arm. We decoupled the motions of the robot arm into a positional and an orientational component, and the geometric constraint equations of each part are found. The equations are the second and the third-order, and their solution is always unique by taking positive roots. For tool-based velocity control, we derived the matrices transforming the velocities of platforms to two or three linear actuators at each parallel mechanism and combined them for the Jacobian considering the geometric constraints of a central axis. The algorithms of the direct kinematics and the Jacobian are successfully implemented in the velocity control of a grinding robot.

The orientational as well as positional workspace of the double parallel robot arm is compared with that of a Stewart platform. The small number of linear actuators installed in the parallel mechanism enlarges the intersection of the area of the workspace, and increases the volume of the workspace by 10% over the Stewart platform. Also, orientations are independently generated at each position since the orientational workspace is decoupled from the positional workspace. This solves a major problem in the workspace of parallel mechanisms which cannot attain a required orientation even at a reachable position. The parallel mechanism of the DPRA reduced the inertia and distributed a load so that the dynamic response is fast and the torques acting at the motors are below 1.6N-m with a payload of 50kg. Therefore, the DPRA can be applied as a robot arm, which requires a wide range of workspace, high stiffness, high ratio of payload to the weight, and low power dissipation.

References

Baron, L. and Angeles, J., 1994, "The Decoupling of the Direct Kinematics of Parallel Manipulators Using Redundant Sensors," *Proc IEEE Int. Conf. Robotics and Automation*, SanDiego, pp. 974~979.

Cheok, K. C. Overholt, J. L, and Beck, R. R, 1993, "Exact Methods for Determining the Kinematics of a Stewart Platform Using Additional Displacement Sensors," *J. Rob. Syst.*, 10 (5), pp. 689~707.

Gosselin, C. 1990, "Determination of the Workspace of 6-Dof Parallel Manipulators," *J. of Mechanism and Design*, pp. 331~336.

Gosselin, C. and Angeles, J., 1990, "Singularity Analysis of Closed-Loop Kinematic Chains," *IEEE Trans. Robotics and Automation*, Vol. 6, No. 3, pp. 281~290,

Lee, M. K., 1995, "Design of a High Stiffness Machining Robot Arm with Double Parallel Mechanism," *J. of KSME* in Korea, Vol. 19 No. 1, pp. 22~37.

Lee, M. K., 1995, "Dynamic Analysis of a Double Parallel Robot Arm," *J. of KSME* in Korea, Vol. 19 No. 11, pp. 2912~2926.

Merlet, J. P., 1993, "Direct Kinematics of Parallel Manipulators," *IEEE Trans. on Robotics and Automation*. Vol. 9, No. 6, pp. 842~846.

Mohamed, M. G. and Duffy, J. 1985, "A Direct Determination of the Instantaneous Kinematics of Fully Parallel Robot Manipulators," *ASME J. of Mechanisms, Transmissions, and Automation in Design*, Vol. 107, pp. 226~229.

Raghavan, M., 1991, "The Stewart Platform of General Geometry has 40 Configurations," *ASME Press in Advances* in Design Automation, pp. 397~402.

Sugimoto, K., 1987, "Kinematic and Dynamic Analysis of Parallel Manipulators by Means of Motor Algebra," *ASME J. of Mechanisms, Transmission, and Automation in Design*, Vol. 109, pp. 3~7.

Zanganeh, K. E. and Angeles, J., 1995, "Real-Time Direct Kinematics of General Six-Degree of Freedom Parallel Manipulators with Minimum-Sensor Data," *J. of Robotic Systems*, Vol. 12. No. 12, pp. 833~844.

Appendix

$$p_1=\frac{3}{2}r_{B1}r_{P1},\ p_2=\frac{1}{2}r_{B1}r_{P1},\ p_3=2cp,\ p_4=\sqrt{3}cpr_{B1},$$

$$p_5=cpr_{P1},\ p_6=r_{B1},\ p_7=\frac{1}{2}\sqrt{3}r_{B1}r_{P1},\ p_8=\frac{r_{B1}}{\sqrt{3}}$$

$$q_1=6r_{B1}r_{P1},\ q_2=8cp,\ q4=4\sqrt{3}cpr_{B1},\ q_5=cpr_{P1},$$

$$q_6=2\sqrt{3}r_{B1}r_{P1},\ q_7=r^2_{P1},\ q_8=4r_{P1},\ q_9=4\sqrt{3}r_{B1}$$

$$c=r^2_{P1}+r^2_{B1}+2cp^2,\ c_s=4cp^2+3r^2_{B1}+3r^2_{P1}$$

$$\begin{aligned}cf_1=&-p_1c\theta_1-p_2c\theta_2+p_3\theta_3c\theta_2+p_4s\theta_1+p_5s\theta_2\\&+p_6\theta_3s\theta_2+p_7s\theta_1s\theta_2+p_8\theta_3c\theta_2s\theta_1+\theta_3^2\\&-cp(-q_1c\theta_1+q_2\theta_3c\theta_2+4\theta_3^2c\theta_2^2+q_4s\theta_1+q_5s\theta_2\\&+q_6s\theta_1s\theta_2+q_7s\theta_2^2+q_8\theta_3c\theta_2s\theta_2+q_9\theta_3c\theta_2s\theta_1\\&+c_s)^{1/2}+c-\theta_{13}^2\end{aligned}$$

$$\begin{aligned}cf_2=&-p_1c\theta_1-p_2c\theta_2+p_3\theta_3c\theta_2-p_4s\theta_1+p_5s\theta_2\\&+p_6\theta_3s\theta_2-p_7s\theta_1s\theta_2-p_8c\theta_2\theta_3s\theta_1+\theta_3^2\\&-cp(-q_1c\theta_1+q_2\theta_3c\theta_2+4\theta_3^2c\theta_2^2-q_4s\theta_1\\&-q_5s\theta_2-q_6s\theta_2s\theta_2+q_7s\theta_2^2+q_8\theta_3c\theta_2s\theta_1\\&+q_9\theta_3c\theta_2s\theta_2+c_s)^{1/2}+c-\theta_{23}^2\end{aligned}$$

$$\begin{aligned}cf_3=&-4p_2c\theta_2+p_3c\theta_2\theta_3-p_4s\theta_1+p_5s\theta_2\\&-2/3p_6\theta_3s\theta_2+\theta_3^2-cp(-q_1c\theta_1+q_2\theta_3c\theta_2\\&+4\theta_3^2c\theta_2^2-q_4s\theta_1+q_5s\theta_2-q_6s\theta_1s\theta_2+q_7s\theta_2^2\\&+q_8c\theta_2\theta_3s\theta_2-q_9c\theta_2\theta_3s\theta_1+c_s)^{1/2}+c-\theta_{33}^2\end{aligned}$$

$$m_1=r_{B2}\cos(\zeta_1),\quad m_2=r_{B2}\sin(\zeta_1),\quad m_3=r_{P2}\cos(\zeta_2)$$

$$\begin{aligned}cf_4=&-(cpc\theta_5)-l_2c\theta_5c\theta_4-m_1s\theta_5+m_2c\theta_5s\theta_4\\&+\left\{cp+\theta_{43}\sqrt{1-\frac{(l_2s\theta_4+m_2c\theta_4-m_3)^2}{\theta_{43}^2}}\right\}\\&\sqrt{1-\frac{(-l_2c\theta_4s\theta_5-cps\theta_5+m_1c\theta_5+m_2s\theta_5s\theta_4-m_3)^2}{\left\{cp+\theta_{43}\sqrt{1-\frac{(l_2s\theta_4+m_2c\theta_4-m_3)^2}{\theta_{43}^2}}\right\}}}\end{aligned}$$

$$\begin{aligned}cf_5=&\,cpc\theta_5-l_2c\theta_5c\theta_4-m_1s\theta_5-m_2c\theta_5s\theta_4\\&-\left\{-cp-\theta_{53}\sqrt{1-\frac{(-l_2s\theta_4-m_2c\theta_4+m_3)^2}{\theta_{53}^2}}\right\}\\&\sqrt{1-\frac{(l_2c\theta_4s\theta_5+cps\theta_5+m_1c\theta_5-m_2s\theta_5s\theta_4-m_3)^2}{\left\{-cp-\theta_{53}\sqrt{1-\frac{(-l_2s\theta_4-m_2c\theta_4+m_3)^2}{\theta_{53}^2}}\right\}}}\end{aligned}$$